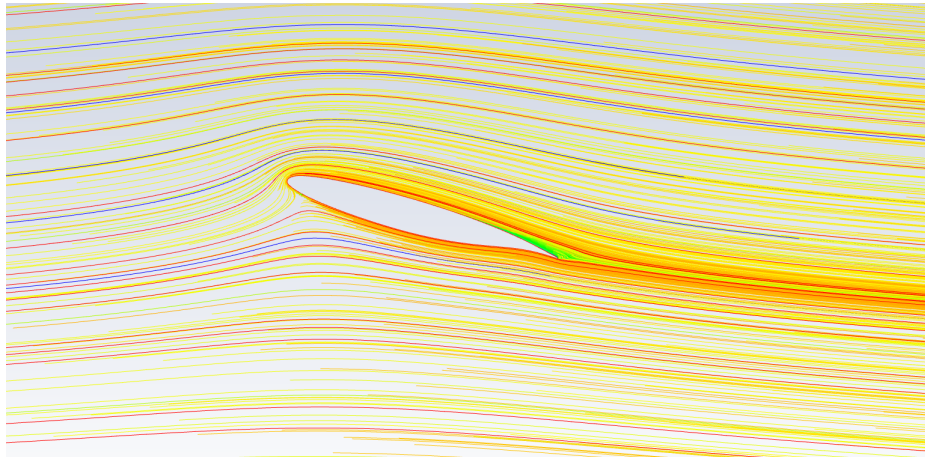# Wing with flow control

SG2224 Applied Computational Fluid Dynamics

Group J3

Parasuram I.V.L.N.
Adrian Stenbäck

Contents

1   Introduction

During the last century the resources spent on aviation research have increased exponentially. Comparing the modern flying vessels of today with the first motorized airplane developed by the Wright brothers shows just how far the development have proceeded. During 2019 alone there was 38.9 millions registered passenger flights which strongly motivates the continuation of aviation research. The drag force and the lift force are two of the most common aspects that are considered when developing an airplane. The drag force acting on a airplane is generated via the friction from the air travelling around the body of the plane and the airplane itself. The drag force highly depends on the velocity of the aircraft and the projected front area of the airplane. In most application the drag force should be minimized in order to for example generate a more fuel efficient airplane. The lift force is the aerodynamic force which makes it possible for the airplane to lift off the ground. The force is generated by a pressure difference between the Leeward and windward side of the airplane wings.

In this project the optimization of the lift force on a D0728 airfoil is investigated. The lift force is increased by placing a small jet in the region of the leading edge of the airfoil. The jet will blow air along the airfoil which will accelerate the flow around the airfoil. The main goal is to accelerate the flow on the leeward side of the airfoil which will lead to an decrease in pressure on the same side. This will in turn lead to a larger pressure difference between the leeward side and the windward side of the airfoil. Increasing the pressure difference leads to an increase in the lift force acting on the airfoil. Further, as the angle of attack increases, the flow separation from the airfoil increases and beyond a critical angle of attack, the flow detaches from the airfoil leading to a loss of lift. Injecting mass (of air here) which is one of the ways to overcome this, helps to add momentum to the flow near the airfoil and thus keeps the flow attached upto a larger angle of attack.

Initially a literature study was performed in order to better understand the subject of Active flow control. In the article "Active flow control applied to an airfoil" by John F. Donovan et al. active flow control is simulated by using a jet on a NACA0012 airfoil. Another paper on related work is "Active control of a stalled airfoil through steady or unsteady actuation jets" bu V. G. Chapin et al. Simulations was carried out with both steady and unsteady jet actuators. In both papers they mange to increase the lift force and delay the angle of attack corresponding to the airfoil stalling.

The influence of the jet was studied with the 3D design software Ansys. A domain around the airfoil was modeled in Ansys computer aided design program Design Modeler and simulations was carried out in Ansys fluid mechanics software Fluent. Basic theoretical motivations suggested that the best position to put the jet was near the stagnation point on the airfoil and that the angle between the jet and the airfoil should be as low as possible. The strength of the jet was determined by considering the flow of mass from the jet into the domain. Various strengths were tested and via interval halving the optimized strength could be determined. Finally simulations with the jet was carried out and the lift coefficient with the jet was compared to the lift coefficient obtained without the jet. Lastly an extensive investigation was carried out to determine how reliable the obtained results were.

2 Method

This section outlines the geometry of the airfoil which was simulated, the domain & boundary conditions used and other simulation settings such as the choice of turbulence model, numerical schemes, etc.
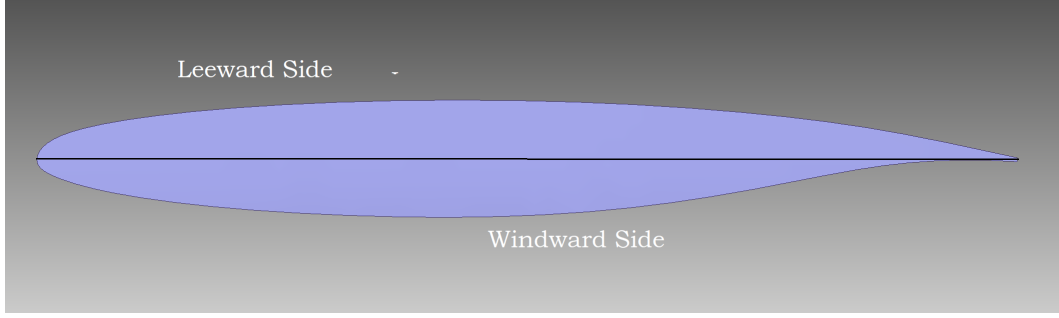
2.1 Geometry & Flow Conditions

Figure 1: DO728 Airfoil

Figure 1 represents the geometry of the airfoil (DO728) which was used in the study. The chord length of the airfoil in 1m. Simulations were performed for a flow with Reynolds number (Re) = 10^7 and free-stream Mach number (M_∞) = 0.2. The Reynolds number is defined based on the chord length of the airfoil. Thus,

$$Re = \frac{LU_\infty}{\nu}$$

where L is the chord length, U_∞ is the free-stream flow velocity, ν is the kinematic viscosity of the fluid (air). The free-stream Mach number is defined based on the free-stream fluid velocity. Thus,

$$M_\infty = \frac{U_\infty}{c}$$

where c is the speed of the speed of sound in the fluid (air)$[c = \sqrt{\gamma RT_\infty}]$. For a given fluid, assuming no large variation in temperature, c is constant and M_∞ is fixed at a specified requirement. Substituting for U_∞ in Re, based on M_∞ and c,

$$Re = \frac{L(M_\infty c)}{\nu}$$

As the fluid properties, Re & M_∞ are fixed, U_∞ needs to adjusted such that it satisfies the mach number and further, the chord length needs to be adjusted such that the Re is achieved. Based, on the requires values, the chord length required is 2.1464 m. The airfoil geometry was scaled by a factor 2.1464 in order to achieve this. The simulation domain is constructed around the airfoil with a space of 15 chord lengths upstream and 25 chord lengths downstream, from the leading edge of the airfoil, along the streamwise direction, and 15 chord lengths on both sides of the airfoil along the transverse direction.
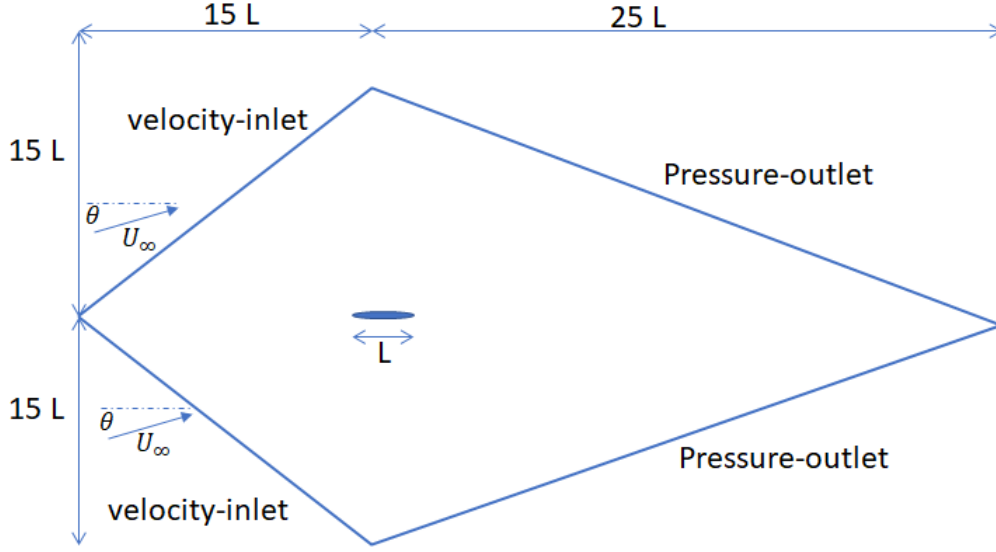
Figure 2: Domain

Fig. 2 depicts the domain along with the boundary conditions used. The velocity inlet at the upstream boundary of the airfoil and the x and y components are input individually to account for the angle of attack. A similar domain is used for all the simulations, with and without mass injections and also flow cases in which the free-stream flow has an angle of attack w.r.t. to the airfoil chord which always oriented along the x-axis. The angle of attack is therefore achieved by keeping the orientation of the airfoil constant and changing the components on inlet velocity.

2.2   Mesh

The geometry and domain as presented in the previous section were meshed in Ansys meshing. A refinement region which is similar in shape to the outer domain geometry was created with a size of 5 chord lengths in the upstream streamwise direction and on both sides of the airfoil in the transverse direction, and 15 chord lengths in the downstream streamwise direction. The airfoil edge was prescribed 2000 edge divisions with biasing so as to have smaller elements closer to the leading edge as the pressure peak occurs close to the leading edge and it is especially important to capture the pressure field well as the lift is the parameter of focus in the current study.

The meshing strategy is more or less similar for the setup with and without mass injection as well. The mesh used is presented in Figs. 3 - 4. More images of the mesh, at different zoom levels and positions are presented in the appendix More Mesh Images

The boundary layer mesh is generated based on the following calculations of the y^+ at the wall:

$$y^+ = \frac{y}{l_*}$$

$$l_* = \frac{\nu}{u_\tau}$$

$$u_\tau = U\sqrt{\frac{C_f}{2}}$$

$$C_f \approx 2 * \frac{0.0296}{Re_x^{1/5}}$$

$$\delta \approx \frac{0.37x}{Re_x^{1/5}}$$

where y is the distance from the airfoil wall in the normal direction, l_* is the viscous wall length scale, ν is the kinematic viscosity of the fluid, u_τ is the wall friction velocity, U is the free-stream velocity, C_f is the skin friction coefficient, Re_x is the local Reynolds number at a x position and δ is the boundary layer thickness. To achieve a target $y^+ = 1$ in order to capture turbulent characteristics well enough through the turbulence models, $y = l_*$, meaning that the first cell height in the boundary layer should be equal to the wall length scale. Further, the total height of the boundary layer mesh should be large enough to cover the boundary layer thickness at that position. Inserting the values of free-stream velocity (U), the scaled chord length for x, and kinematic viscosity (ν) as 68.05 m/s, 2.1464m, 1.4607e-05 m^2/s respectively yields $\delta = 0.0316m, C_f = 0.0024$. This further gives $u_\tau = 2.3360m/s, l_* = 6.253e - 06m$. Thus, the first cell height, which should be equal to l_* in order to result in $y^+ = 1$ should be around 6.25e-06 m. This was implement in the inflation layer meshing in Ansys. A smaller first layer height was used in the inflation to account for any possible errors. The resulting y^+ was later checked after running the simulation, and it is as presented in Fig. 5. The wall y^+ value was plotted against the x-position along the airfoil. It was observed that Throughout the airfoil geometry, the y^+ value does not exceed 1, which is favourable.
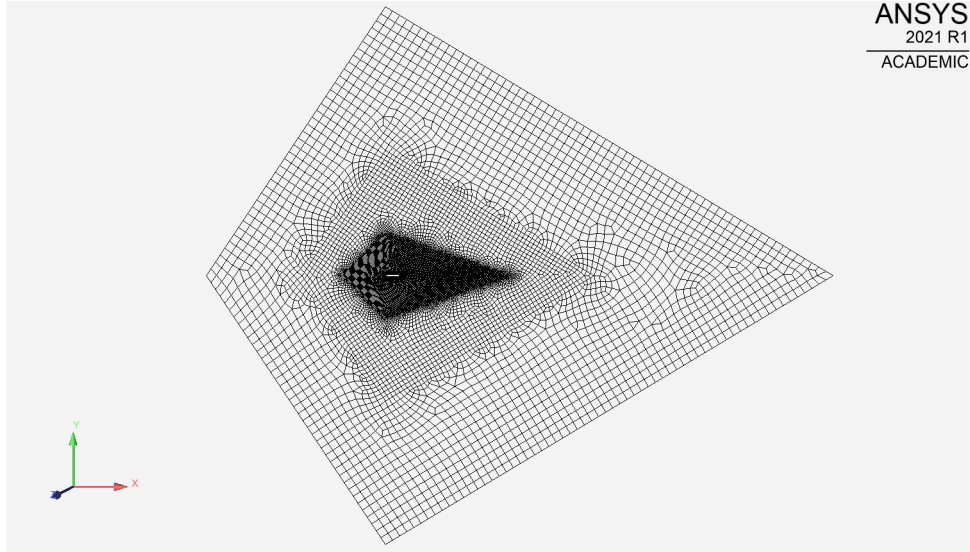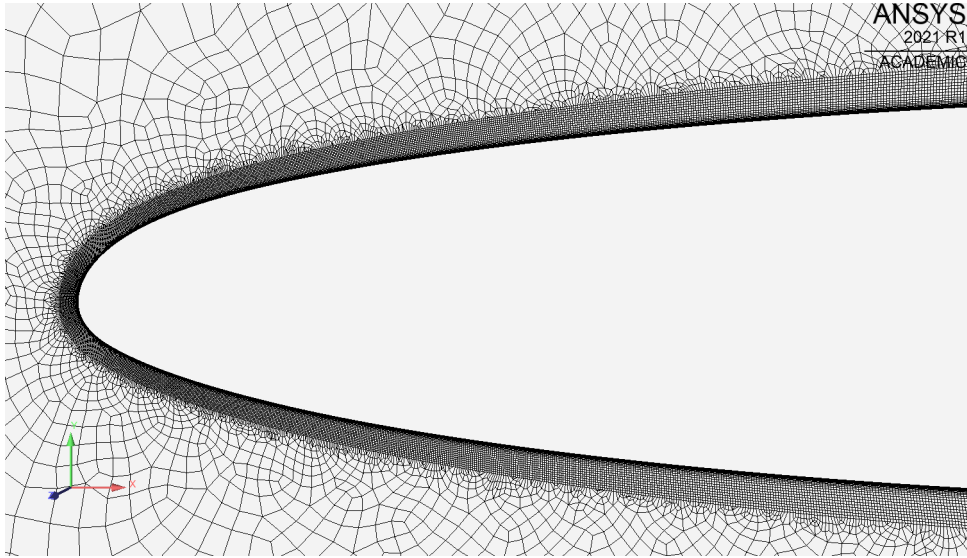
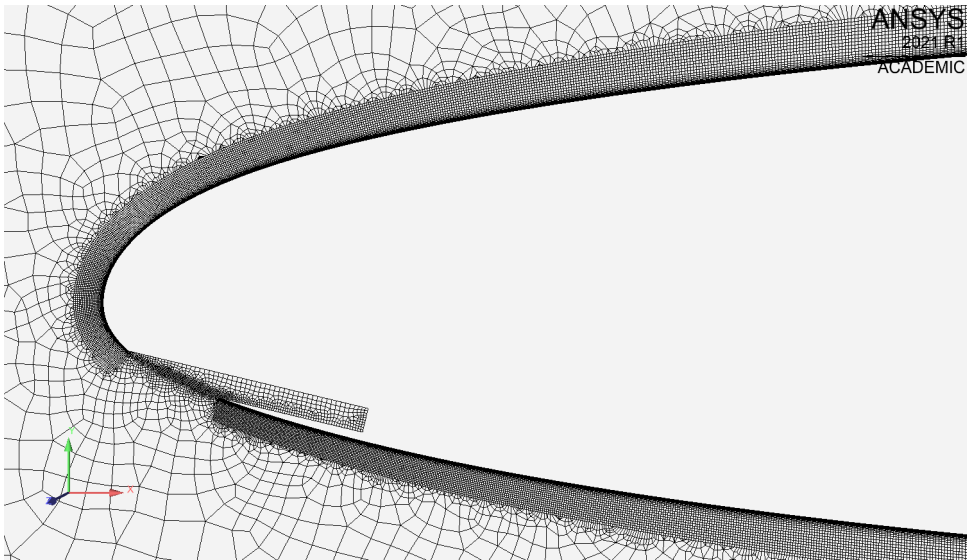Figure 3: Mesh of geometry without mass injection

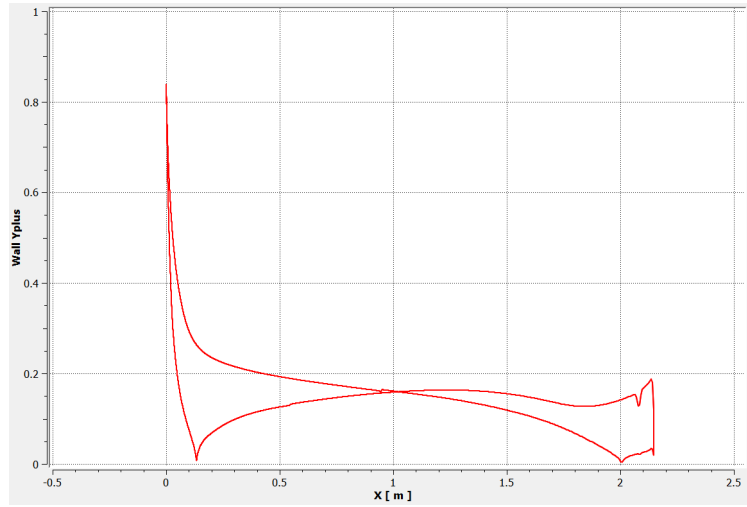Figure 4: Mesh of the geometry with mass injection

Figure 5: y + as a function of the x position along the airfoil.

The quality of the mesh generated was also checked based on the skewness and the orthogonal quality metrics. The desired values of these parameters for a good mesh are 0 and 1 respectively. These variation of these metrics across the domain is plotted as contours and presented in Fig. 6 & 7 respectively. It can be seen that these parameters do not deviate much from the ideal values by a large magnitude. However, the goodness of the mesh for this flow setup cannot be judged solely on these parameters as it also depends on the orientation of the mesh along the gradients and the numerical scheme along with it would be used as it determines the dispersion and dissipation errors of the numerical scheme.
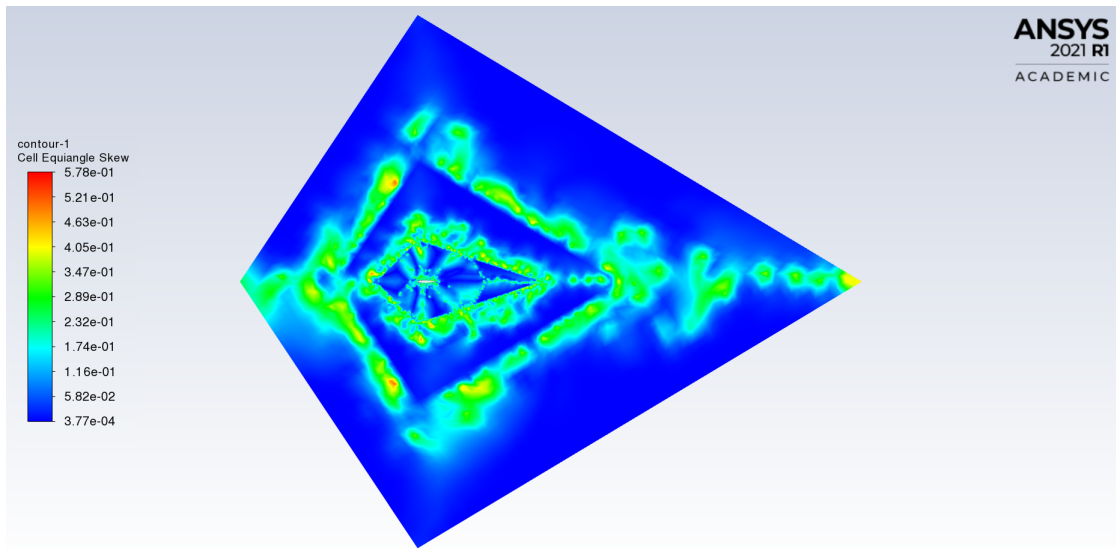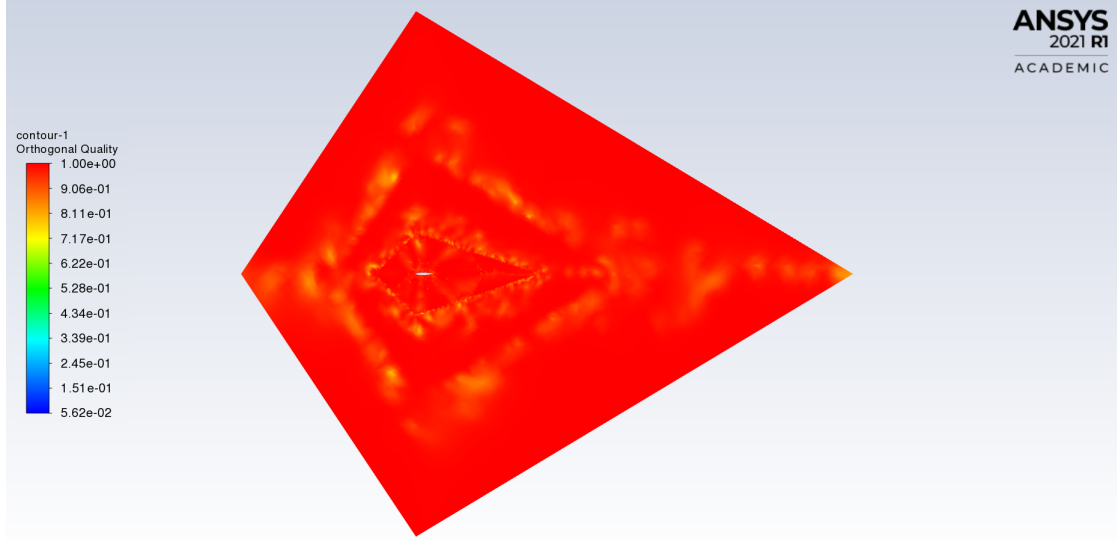

Figure 6: Mesh skewness contour

8

Figure 7: Mesh orthogonality contour

2.3 Solver

A pressure-based, steady state solver was used for the simulations along with $k - \omega$ SST turbulence model. As the flow conditions are at the boundary of compressible flow, thus being weakly compressible, the energy equation was also solved in addition to the mass and momentum conservation equations. The fluid medium is considered to be air, with the default properties at room temperature. The pressure-velocity coupling was chosen as *Coupled* along with II order schemes for all the fluxes (pressure, momentum, k, etc.). The condition for convergence of residuals was set at $1e - 06$ for all the properties, i.e. mass, x-velocity, y-velocity, k, ω, energy. In addition to monitoring the residuals, it was also ensured to check the variation of lift and drag as residuals alone may not be enough to know the correctness of the solution. The simulation was run further until the lift and drag achieved steady values even if the residuals converged before. As the flow behaviour needs to be steady based on the assumption of this study, the lift and drag are not expected to vary with iterations.

Fig.8 presents the variation of the residuals with iteration for the flow case with no mass injection and zero angle of attack. The residuals steadily decrease without any oscillations and the lift and drag also stabilised before the convergence of residuals, increasing the confidence in the results.

9
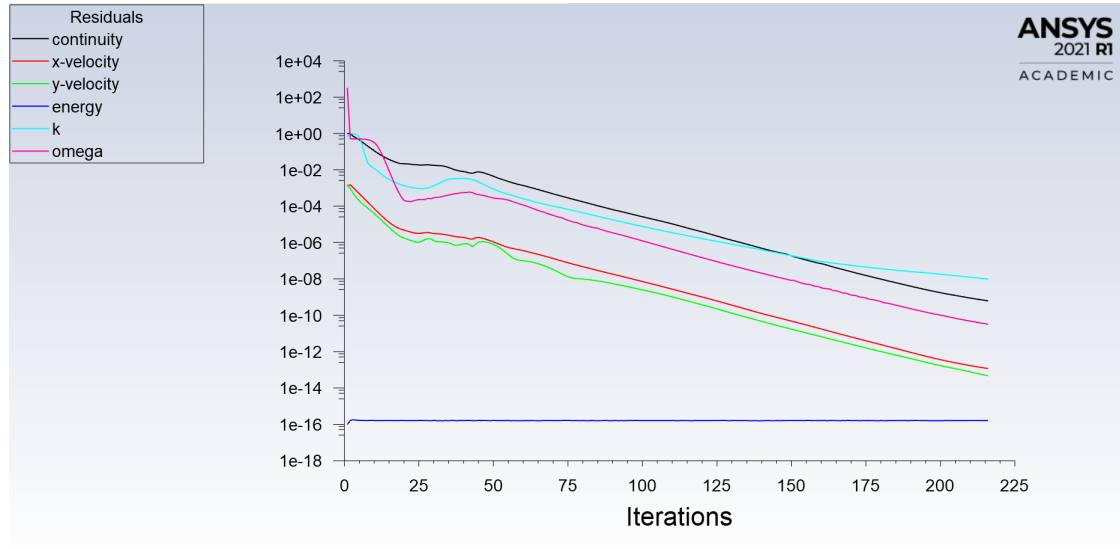
Figure 8: Variation of residuals with iterations

2.4 Jet

The Jet was implemented as a small pipe emerging from the inside of the airfoil. Based on results from previous studies the pipe dimension was set to 20 mm x 5 mm. In order to determine a good position to the jet the project supervisor was consulted, he suggested that the jet should be positioned close to the stagnation point of the airfoil but closer to the leading edge than the stagnation point itself. Using the angle of attack corresponding to the maximum lift without the jet the stagnation point was found.

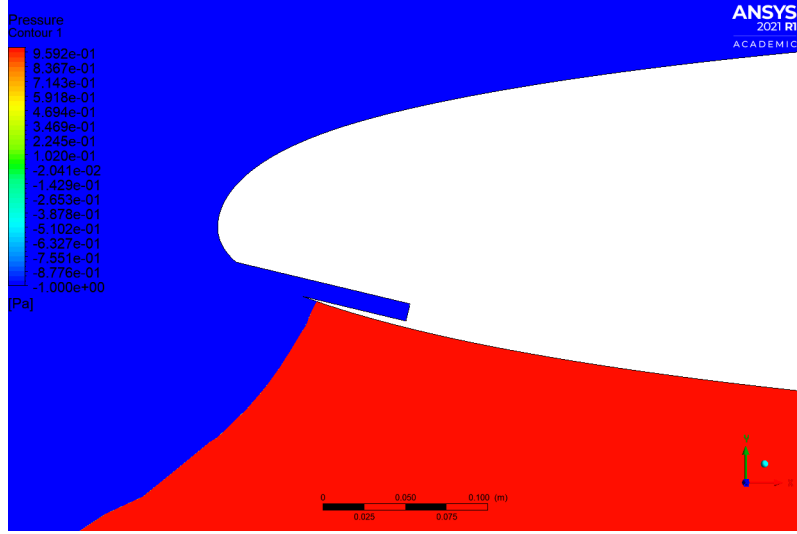Figure 9: Visualisation of stagnation point after adding the jet.

As seen in Fig. 9 the stagnation point is located where the red and blue region meet on the airfoil and the jet is positioned on the left side of the stagnation point. Since the flow will be tangential to the surface of the airfoil it is beneficial to set the angle between the surface of the airfoil and the jet as small as possible. This will minimize the deceleration of the flow traveling on the right hand side of the jet when it reaches the jet. Instead it will be fully accelerated. The last thing to address in the implementation of the jet was the mass flow rate, how much mass should be injected? If to much is injected the flow will detach from the airfoil since the jet will be to strong. At the same time one wants to maximum the lift which means that the injected mass flow rate can't be to low. In order to address this the blowing momentum coefficient was used which is defined as,

$$C_\mu = \frac{\dot{m}U_j}{0.5\rho_\infty U_\infty^2 L} \tag{1}$$

$\dot{m}$ is the mass flow, U_j is the exit velocity of the jet, L is the cord length of the airfoil. The blowing momentum coefficient was set to two extreme values 0.01 and 0.1. Then the bisection method was used which meant that simulations was carried out for 0.01 and 0.1. The solution corresponding to $\dot{m} = 0.01$ converged and the solution corresponding to $\dot{m} = 0.1$ did not. In order to find the mass flow rate which corresponded to the largest lift the interval was divided in half and a new simulation with $\dot{m} = 0.05$ was carried out. This procedure was repeated until a maximum was found that converged.

3 Results

3.1 Lift and Drag

The following section outlines the obtained lift coefficient for various angles of attack with and without the jet.
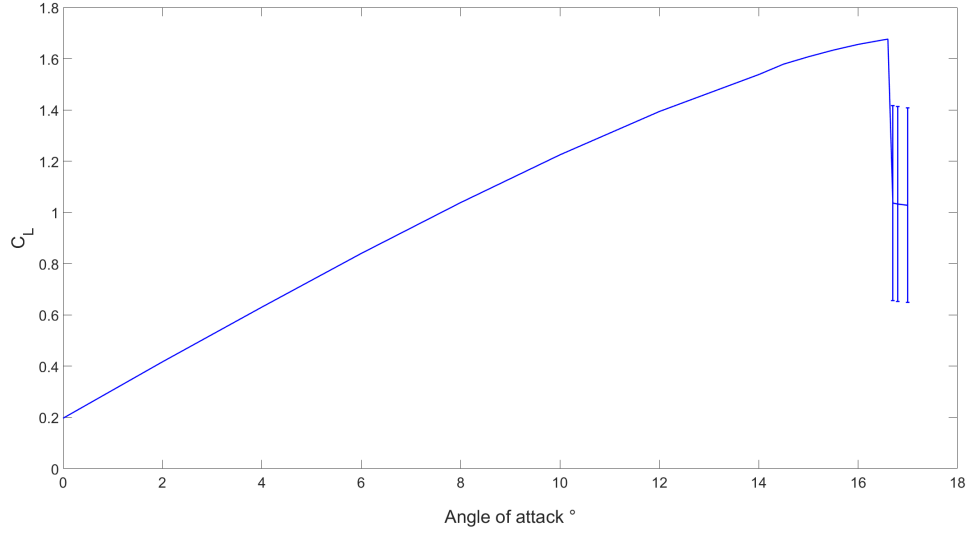
Figure 10: Lift coefficient as function of angle of attack without jet

Fig. 10 shows how the lift coefficient increases as the angle of attack increases. The maximum lift was obtained at the angle of attack equal to 16.6°. The lift coefficient itself was calculated to 1.68. For angles of attack above 16.6 degrees the solution did not converge, instead the lift oscillated heavily around a lift coefficient equal to 0.1. In order to represent this in a correct matter an mean and standard deviation was calculated over the last 1000 iterations of the simulation. These values are represented in Figure 10 as error bars. However it should be pointed out that the solution is not physical. It is just an indication of an decrease in lift.
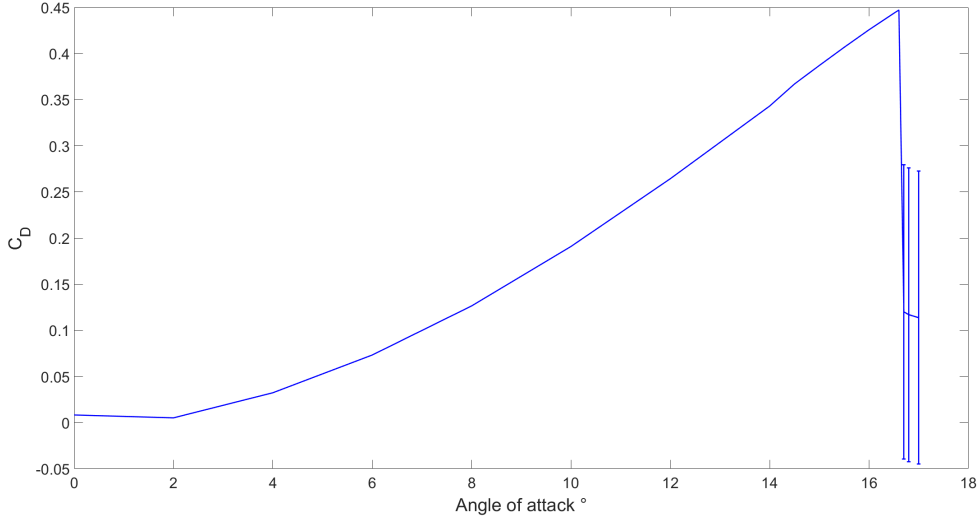
Figure 11: Drag coefficient as function of angle of attack without jet

The drag coefficient as a function of the angle of attack in Figure 11, shows how the drag is increasing as the angle of attack is increase which is expected since the projected are of the airfoil will increase as the angle of attack increases. Since the solution did not converge the drag is also represented with an error bar for angle of attack larger than 16.6°. Here one can see the nonphysical solutions since the error bars indicate that the drag can be negative which is not physical at all.

3.2   Mass flow rate

The table bellow shows the lift and drag forces obtained for the C_μ:s where the solution converged. Using the bisection method as mentioned above the mass flow rate corresponding to the highest lift was found and it was equal to $\dot{m} = 0.025$.

C_μ	Lift force [N]	Drag force [N]
0.01	11198.97	3263.8436
0.025	12716.23	3959.5848

Table 1: Reported lift and drag force for different C_μ.

The affect of the jet was evaluated as the increase in lift and also how much the stall was delayed after the implementation of the jet. New simulations was executed for various angles of attack and the result was compared to the results obtained for the airfoil without the jet.
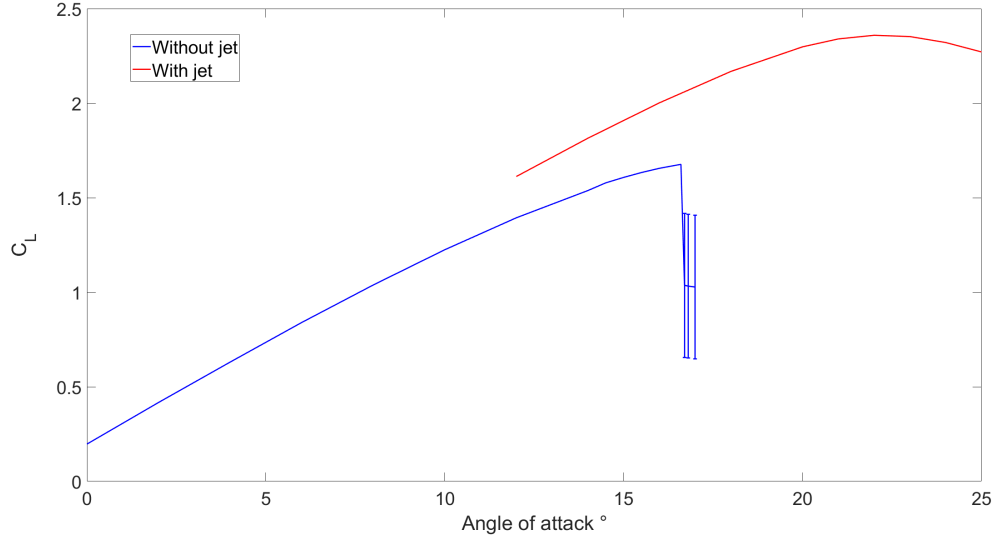
13

Figure 12: Lift coefficient as function of angle of attack with jet

In Figure 12 the lift curve obtained with the jet is plotted together with the curve obtained without the jet. The lift coefficient obtained with the jet is larger for all angles of attack compared to the airfoil without the jet. The maximum lift coefficient for the airfoil with the jet was calculated to 2.36 and was obtained at an angle of attack equal to 22°. The figure also shows how the maximum lift is obtained for a larger angle of attack, which implies that the stall has been delayed from 16.6° to 22°. Also worth noting is the fact that without any change in the solver, mesh etc the solution was able to converge after the point of stall was reached. This can be explained by the fact that the flow separation is different when the the jet is implemented compared to when it is not. This difference can be highlighted by considering the path lines for the simulations with and without the jet, see section 3.3.
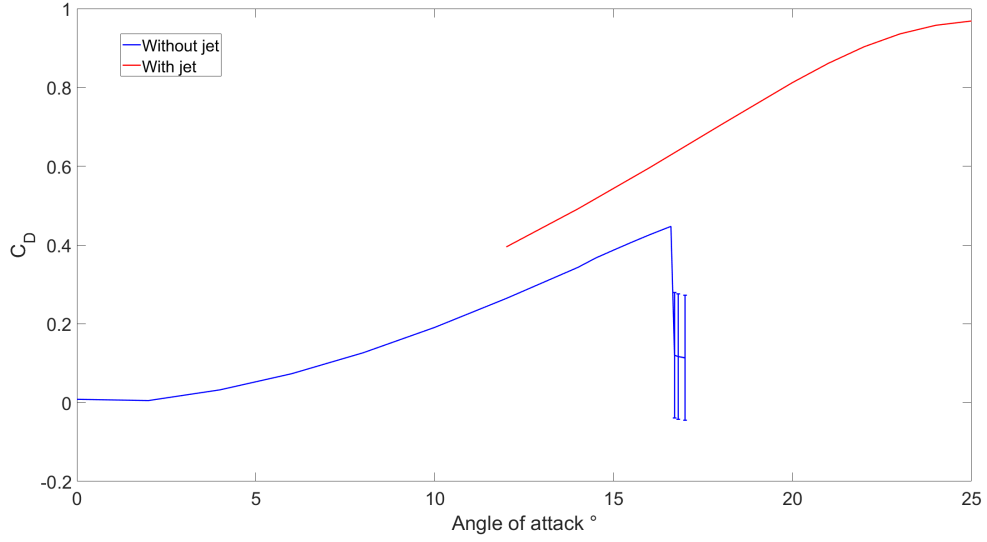
Figure 13: Drag coefficient as function of angle of attack with jet

Regarding the drag of the airfoil with the jet Figure 13 shows how the drag also is larger at every angle of attack. The drag also increases as the angle of attack increases which again is expected.

3.3 Flow visualisation

In order to investigate if the flow separate differently when the jet is implemented compared to when it's not implemented the path lines for two simulations was plotted. For the case without the jet the path lines from a simulation with angle of attack equal to 17° was used and for the case with the jet implemented a simulation for angle of attack equal to 25° was used. Note that in both of these simulations the flow have separated from the airfoil.
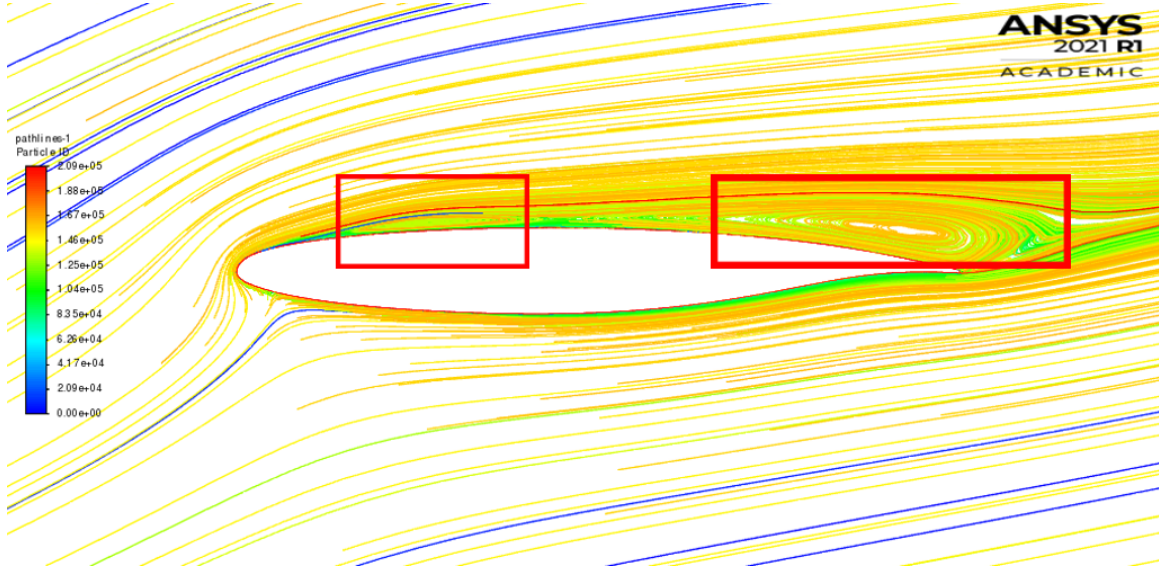
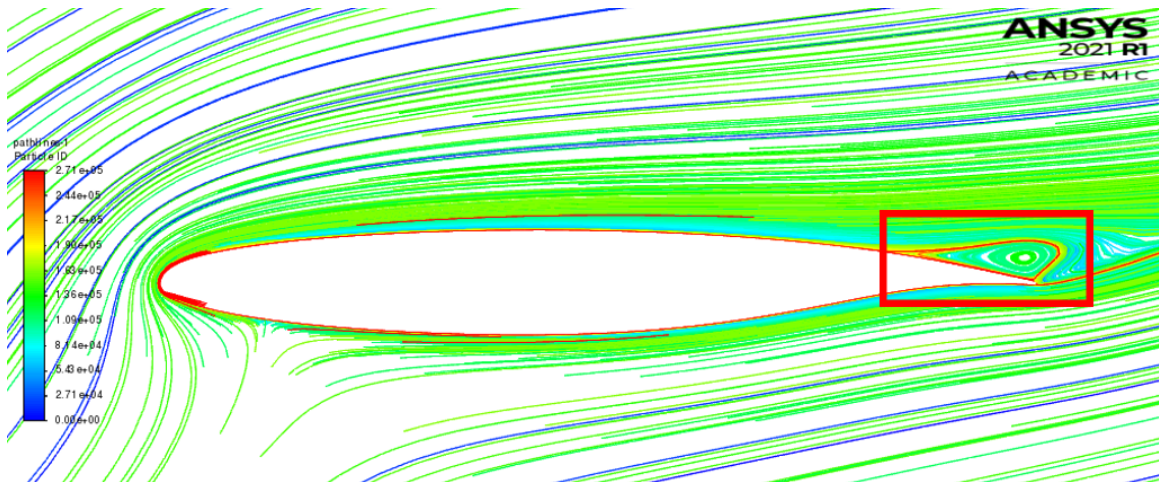Figure 14: Path lines for simulation without jet with angle of attack equal to $17°$

Figure 15: Path lines for simulation without jet with angle of attack equal to $25°$

Fig. 14 shows how at the leading edge the flow has detached from the airfoil and particles are travelling in circles in a vortex. Which means that without the jet the airfoil experience leading edge separation which means that the lift will have an abrupt decrease. On the other hand Fig. 15 is quite different. There is no vortex forming at the leading edge, instead it seems like separation occurs at the trailing edge. This kind of separation is not as abrupt as the leading edge separation instead the lift decreases somewhat as can be seen in Fig. 12. This could also be an explanation to why the solution is not able to converge without the jet for angle of attack larger than $16.6°$ which the solution is able to do when the jet is implemented.

4 Reliability of Results

One of the most important aspects if not the most important, that needs to be addressed when assessing a CFD simulation is if the results that have been obtained is reliable. Since the approximations of the implementation of the jet and the jet itself is quite rough in this project the main focus have been on evaluating the reliability of the results, rather than trying to optimize the maximum lift coefficient obtained with the jet. The reliability of the results has been evaluated by a number of different approaches which will be presented below.

4.1 Mesh Convergence

As a first to step to establish the reliability of the simulation results, a mesh convergence study was performed. This exercise establishes that the mesh size doesn't affect the solution as the mesh is not a physical entity and thus should not influence the flow. Three different meshes were prepared in addition to the mesh that was used in the rest of the study (where the effect of mass injection, variation with angle of attack and variation with mass injection coefficient were examined). The mesh which was used for the rest of the study, which we'd refer to main mesh had approximately 125000 nodes. Among the three other meshes, one is a finer mesh, with around 260000 nodes and two others were coarser meshes with around 90000 and 70000 nodes. The simulation were performed on these different meshes, keeping all other settings the same for a setup with no mass injection and zero angle of attack flow, and the lift coefficient was compared, as that is the parameter of most importance in this study overall. The lift coefficient from all the meshes is compared against the result from the finest mesh, as it is generally expected that finer mesh would capture the flow field better, and % error in lift coefficient from this comparison is plotted in Fig. 16
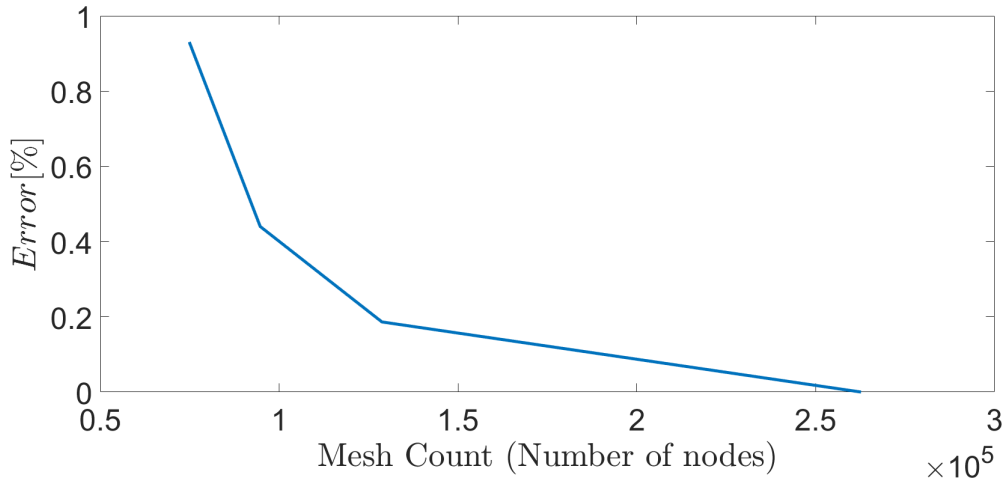

Figure 16: Variation of percentage error in lift coefficient with mesh size

4.2 Domain size convergence

The effect in changes of the size of the grid was investigated by constructing two new domains. The first domain was obtained by removing 10 chord lengths in the stream wise direction and the transverse direction from the domain presented in Fig. 2, i.e the new domain was 30 L in the stream wise direction and 20 L in the transverse direction. In the same way a larger domain was obtained by adding 10 chord lengths in each direction which meant that the large domain was 50 L in the stream wise direction and 40 L in the transverse direction. Simulations was carried out with zero angle of attack and without the jet, the results are presented in table 2.

Domain	Lift force [N]	Drag force [N]	Max iteration
Small	1222.98001	50.53120	127
Original	1222.98232	50.53568	127
Large	1222.98562	50.53789	127

Table 2: Results from domain size simulations

As seen in Tab 2 the results in terms of lift force and drag force is very similar. Both the lift and the drag forces are exactly the same up to the third decimal and on top of that all simulations converged at the same iteration. Also worth mentioning is that the residuals minimum limit was set to 1e-6 in each simulation. Due to the almost exact result from each simulation it is safe to say that the effect of the size of the domain has little influence on the obtained solution which is positive since it implies that the size of the grid is favorable.

4.3 Solver settings

4.3.1 Turbulence Model

To investigate how different Turbulence models might affect the solution obtained in section 3 three different turbulence models were used in four different cases. The four cases was zero angle of attack with no jet, 16.5° of angle of attack with no jet, no angle of attack with jet and 22° of angle of attack with jet. The turbulence models used were first of all the k-omega model which was used in the original simulation, the k-epsilon model and the Spalart-Allmaras model.

Unfortunately none of the simulations using the k-epsilon model converged which is why all the corresponding values have been left as blank in the following tables.

Model	Lift force [N]	Drag force [N]
k-epsilon	-	-
k-omega	1222.9703	50.530899
Spalart-Allmaras	1233.4615	55.845848

Table 3: Results obtained for various turbulence models without a jet and zero angle of attack.

Table 3 shows how the lift force and the drag force for the k-omega model and the Spalart-Allmaras model is very similar for the case with the zero angle of attack and no jet. There is a small difference of around 11 newton in the lift force and an even smaller difference of around 5 newtons in the drag

force. Table 4 on the other hand shows how the difference in the obtained solutions increase for 16.6° angle of attack for both lift and drag. In this case the lift and drag differs around 550 newton and 193 newton respectively.

Model	Lift force [N]	Drag force [N]
k-epsilon	-	-
k-omega	10187.606	2701.681
Spalart-Allmaras	9637.4119	2508.2489

Table 4: Results obtained for various turbulence models without a jet and 16.6° angle of attack.

However the solutions still agree well and of course the flow will get far more turbulent with the larger angle of attack which means that the simulation will be more chaotic and it will be harder to capture the characteristics of the flow. So it makes sense that the difference in this case would increase compared to the case with zero angle of attack.

Model	Lift force [N]	Drag force [N]
k-epsilon	-	-
k-omega	1692.9044	349.01259
Spalart-Allmaras	1533.9784	283.19885

Table 5: Results obtained for various turbulence models with a jet and zero angle of attack.

Table 5 shows how after the implementation of the jet the difference in lift between the models for no angle of attack have increased compared to the values reported in table 3. The difference is now around 160 N instead of 11 newtons as reported above. The difference in the drag force has also increased compared to the case with no jet.

Model	Lift force [N]	Drag force [N]
k-epsilon	-	-
k-omega	14364.094	5499.7501
Spalart-Allmaras	14020.764	5363.901

Table 6: Results obtained for various turbulence models with a jet and 22° angle of attack.

For maximum angle of attack the difference between the models have decreased compared to the difference between the models for maximum angle of attack without the jet. One explanation could be the same reason as mentioned above regarding the difference in separation. The separation occurring when the jet is present is easier to model which means that the difference between the turbulence models will decrease.

4.3.2 Coupling Schemes

Another test of the reliability of the results was to check suitability of the numerical schemes used for the flow setup under consideration. The Coupled scheme was used for pressure-velocity coupling along with II order upwind discretization of all the parameters such as pressure, velocity, k, ω, energy for the simulations in general. Simulations were performed with SIMPLEC and PISO schemes

with II order discretization as earlier, on the flow past airfoil with and without mass injection, at 0 angle of attack and the angle of attack which gives maximal lift in each case. i.e. 16.5° for no mass injection and 22° for mass injection. Further, the influence of order of discretization was tested by performing simulations of the airfoil without mass injection at 0° and 16.5° angle of attack. The angles of attack for the studies under this section were chosen as they represent the extreme ends of the changes in the flow behaviour, as the flow tends towards separation and unsteadiness as the angle of attack increases.

It can be seen from the results that the lift as well as drag forces are very similar with all the coupling schemes in the case of no mass injection for both angles of attack. However, when mass is injected, the forces vary slightly for no angle of attack. For the large angle of attack with mass injection, the forces match quite well between Coupled and SIMPLEC, but it was not possible to obtain a converged solution with the PISO scheme even after 10000 iterations. It can further noticed that the Coupled scheme took significantly lesser number of iterations to obtain a converged result as compared to the other two schemes. A possible reason for this could the sensitivity of these schemes to skewness of the mesh and neighbour correction.

Schemes	Lift force [N]	Drag force [N]	Max iteration
Coupled	1222.83	50.53	125
SIMPLEC	1218.73	50.57	1500
PISO	1216.34	50.45	9000

Table 7: Results obtained for different schemes without a jet and 0 angle of attack.

Schemes	Lift force [N]	Drag force [N]	Max iteration
Coupled	10187.61	2701.68	480
SIMPLEC	10183.48	2700.32	10500
PISO	10174.039	2697.15	9500

Table 8: Results obtained for different schemes without a jet and 16.5° angle of attack.

Schemes	Lift force [N]	Drag force [N]	Max iteration
Coupled	1692.78	349.03	110
SIMPLEC	1451.20	402.37	9000
PISO	1484.31	390.25	3000

Table 9: Results obtained for different schemes with a jet and 0 angle of attack.

Schemes	Lift force [N]	Drag force [N]	Max iteration
Coupled	14373.043	5503	150
SIMPLEC	14366	5500.46	6800
PISO	-	-	-

Table 10: Results obtained for different schemes with a jet and 22° angle of attack.

20

4.3.3 Order of schemes

In addition to checking different pressure-velocity coupling, the influence of order of discretization was also checked for the setup without mass injection for 0° and 16.5° angle of attack, with the Coupled scheme. It can be seen that the II order and III order schemes produce almost identical results while first order schemes deviates a bit. A possible reason for this could be due to smearing out of the flow field due to the I order discretization. The trends are similar for the higher angle of attack as well. Further, in comparison to the different schemes, all the cases take similar number of iterations to converge. It is reasonable as the order of the discretization has greater influence on the accuracy on the solution that the convergence of the solution itself. This further tells us that the convergence of residuals alone may not be the criteria for assessing a solution.

Order of schemes	Lift force [N]	Drag force [N]	Max iteration
I order upwind	1163.572	91.98	125
II order upwind	1222.83	50.53	125
III MUSCL	1217.51	50.45	125

Table 11: Results obtained for different schemes without a jet and 0 angle of attack.

Order of schemes	Lift force [N]	Drag force [N]	Max iteration
I order upwind	9594.80	1963.86	170
II order upwind	10187.61	2701.68	480
III MUSCL	10122.05	2682.47	280

Table 12: Results obtained for different schemes without a jet and 16.5 angle of attack.

4.4 Rotating the body vs Diamond domain

Finally, to check if the approach of keeping the airfoil orientation constant and changing the velocity components to simulate angle of attack instead of actually rotating the body resulted in any changes a few angles of attack were simulated by rotating the geometry without mass injection with the domain size used along the transverse direction, the inlet boundary remains intact for all the angles upto stall, which can be simulated with a steady, 2D setup. Fig. 17 presents the error in percentage between solution with rotated body and diamond mesh as a function of the angle of attack. It can be noticed that difference is fairly low, and increases with angle of attack, which is reasonable as the need for the diamond approach becomes more important at higher angles of attack.
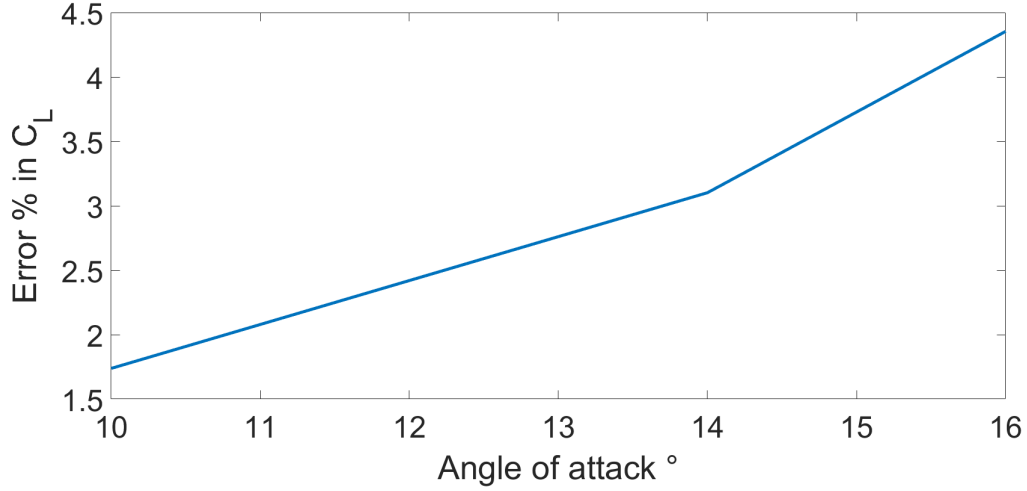
Figure 17: Error in percentage between solution with rotated body and diamond mesh as a function of the angle of attack

5 Conclusion

In this project the possibility of increasing the lift coefficient of an airfoil with the help of a small jet has been investigated. An attempt of optimizing the jet in terms of position, angle and mass flow rate has been made. Simulations for various angles of attacks have been carried out with and without the jet. The results shows that the maximum lift can be increase and that the angle of attack where the airfoil stalls can be delayed. The results also showed that the jet affects how the flow is detached from the airfoil when it reaches stall. Without the jet it seems like the flow detaches at the leading edge and with the jet the flow seems to detach at the trailing edge. Since leading edge separation often is associated with a large decrease in lift the jet improves the separation characteristics of the airfoil. The reliability of the results was investigated with various tests which all showed that the results should be considers as reliable. The only indication of unreliable results is the fact that the solution wasn't able to converge when the k-epsilon turbulence model was used. However a possible explanation is that the k-epsilon model is often used for free-shear layer flows with small pressure gradients and also for confined flows.

6 References

[1] Active flow control applied to an airfoil" by John F. Donovan et al

[2] Active control of a stalled airfoil through steady or unsteady actuation jets" bu V. G. Chapin et al.
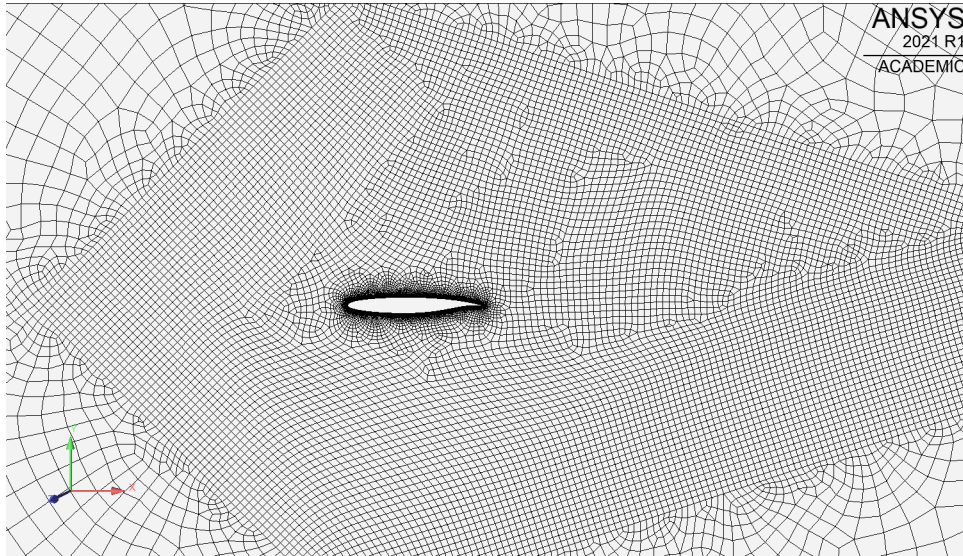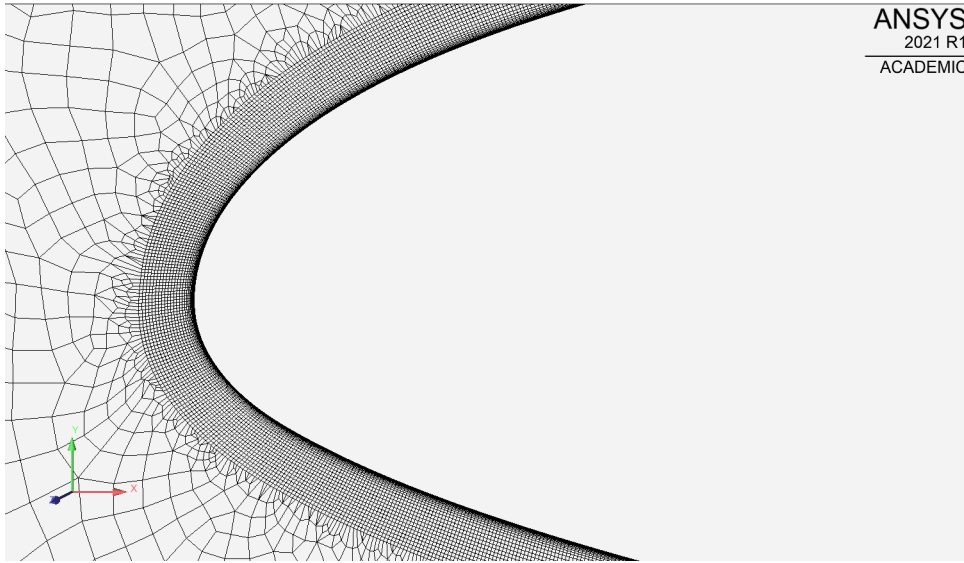
Appendix

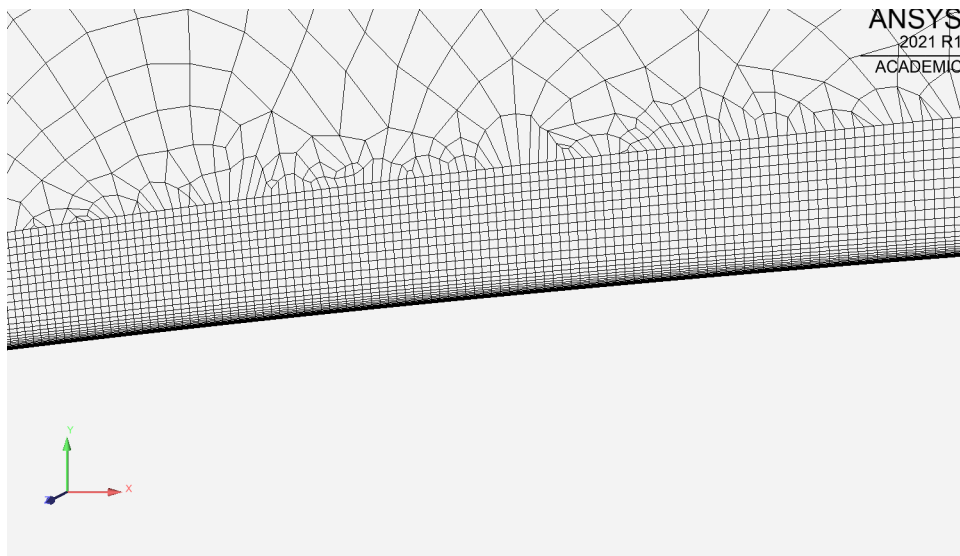## Mesh

Figure 18: Caption

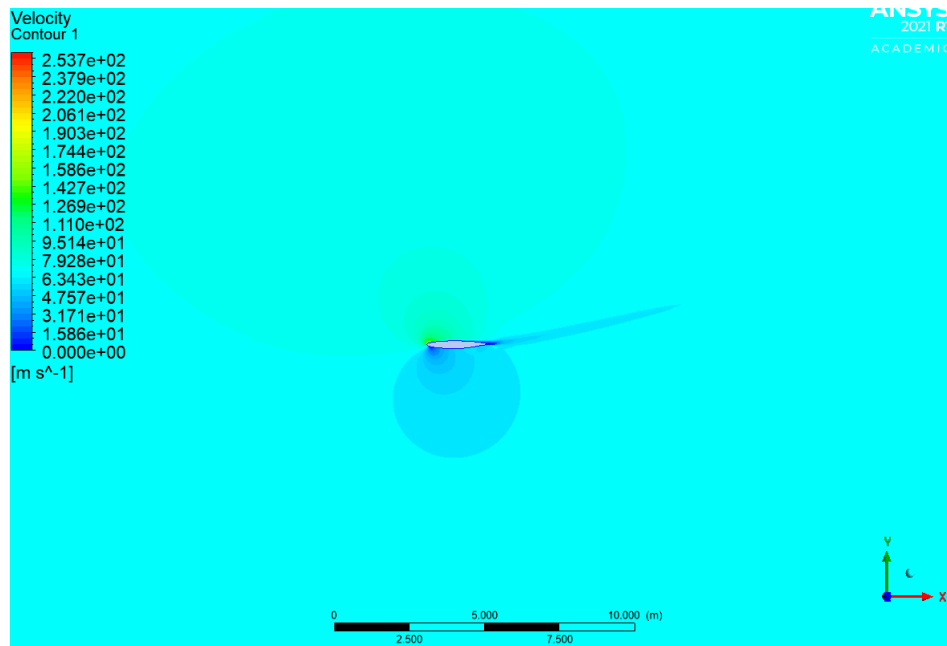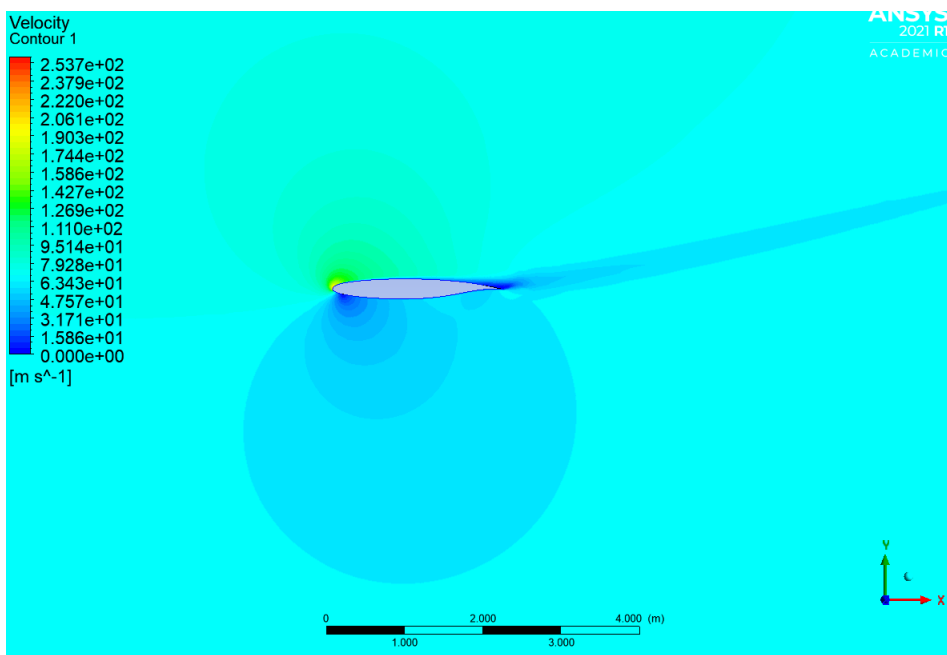Figure 19: Caption

Figure 20: Caption

Velocity fields

Figure 21: Velocity field for 16.5° angle of attack without jet.

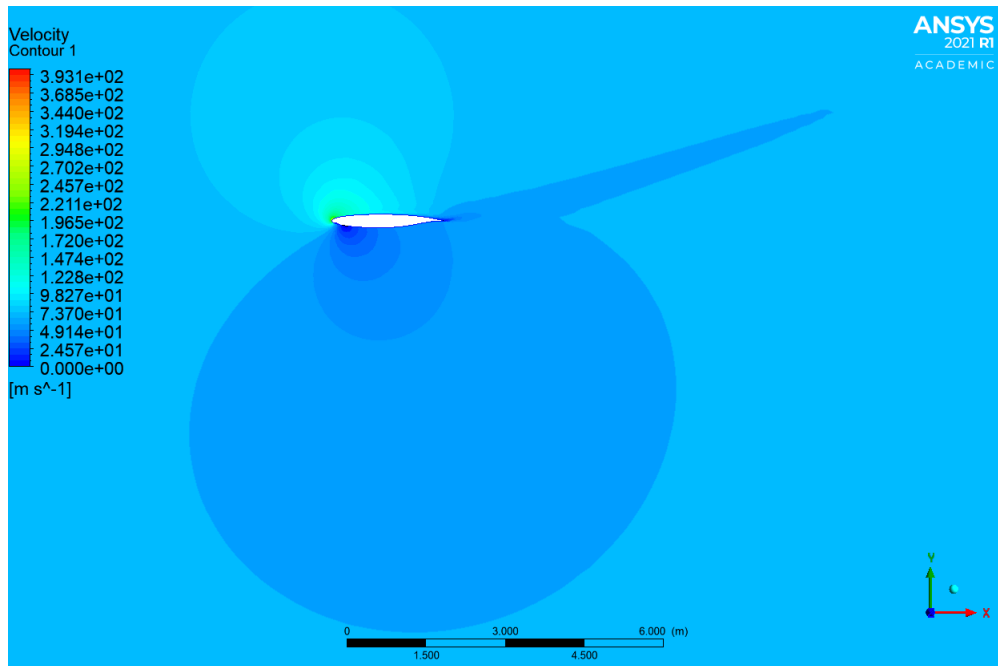Figure 22: Velocity field for 16.5° angle of attack without jet.
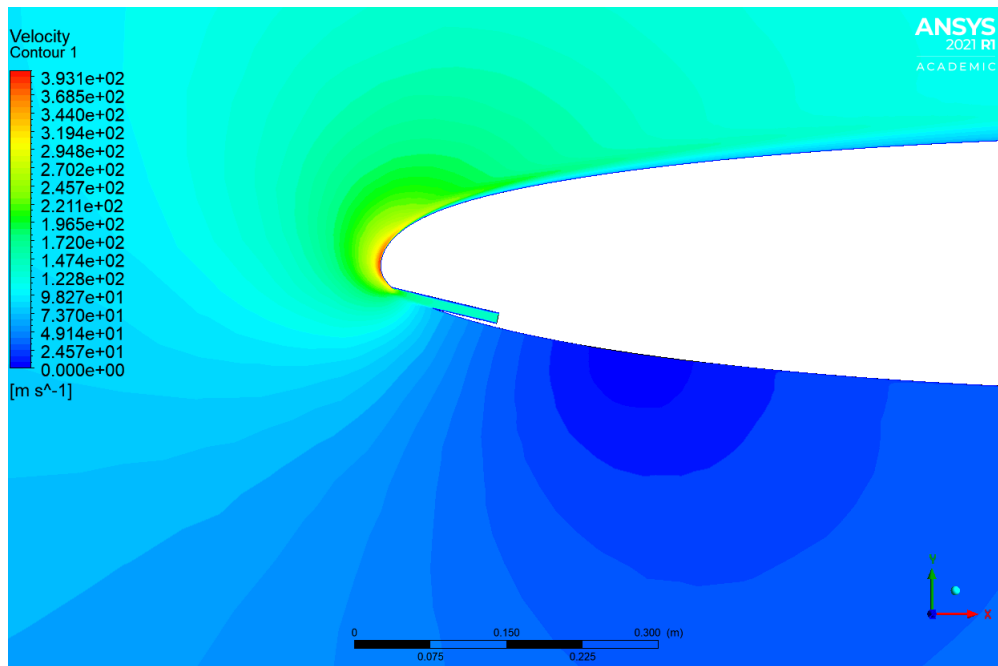
Figure 23: Velocity field for 22° angle of attack with jet.

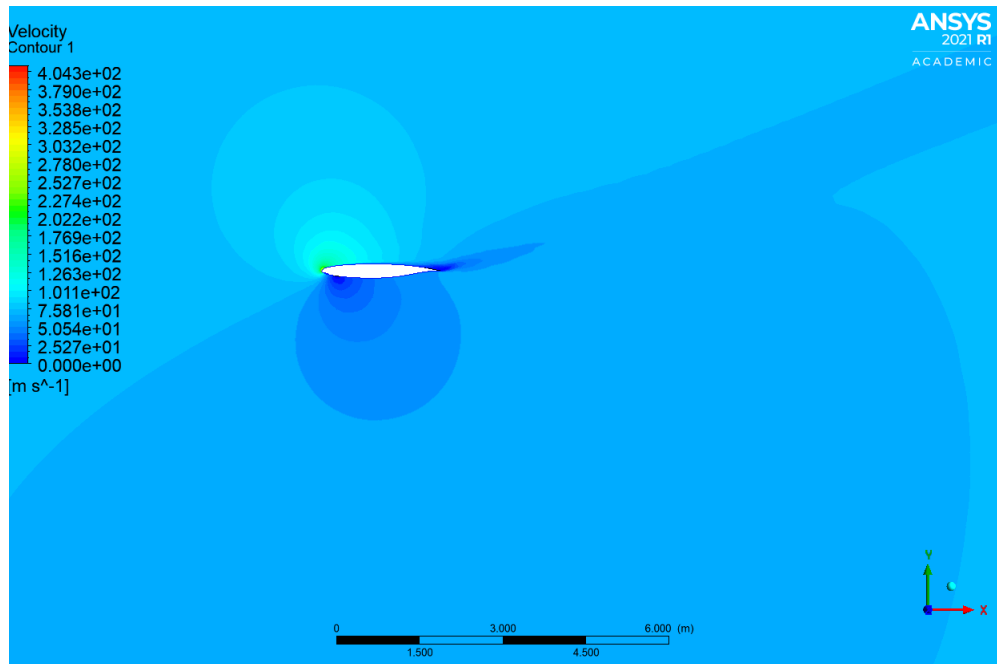Figure 24: Velocity field for 22° angle of attack with jet.

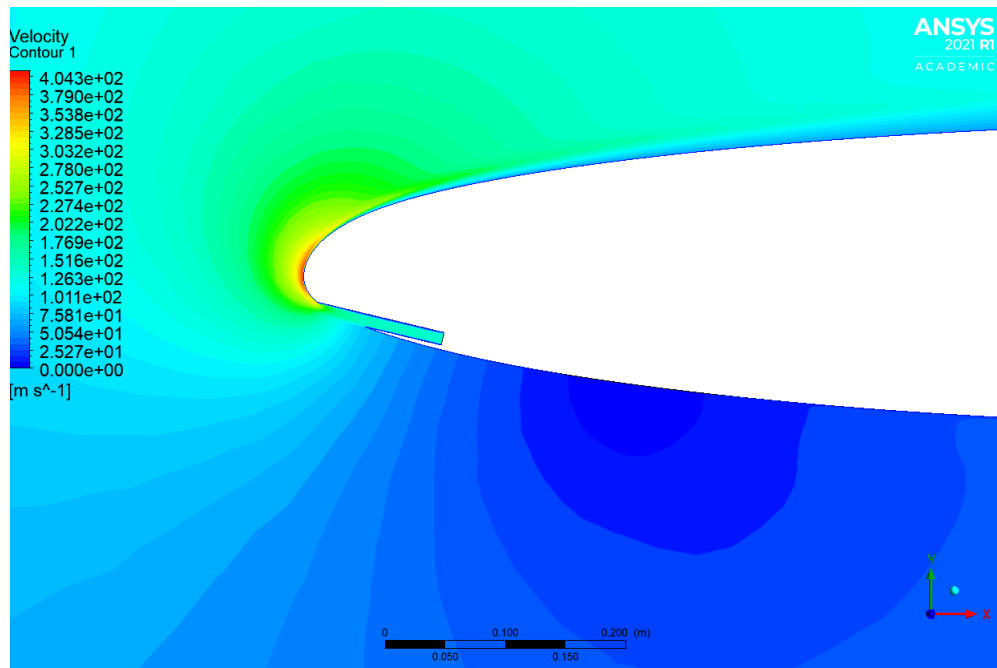Figure 25: Velocity field for 26° angle of attack with jet.

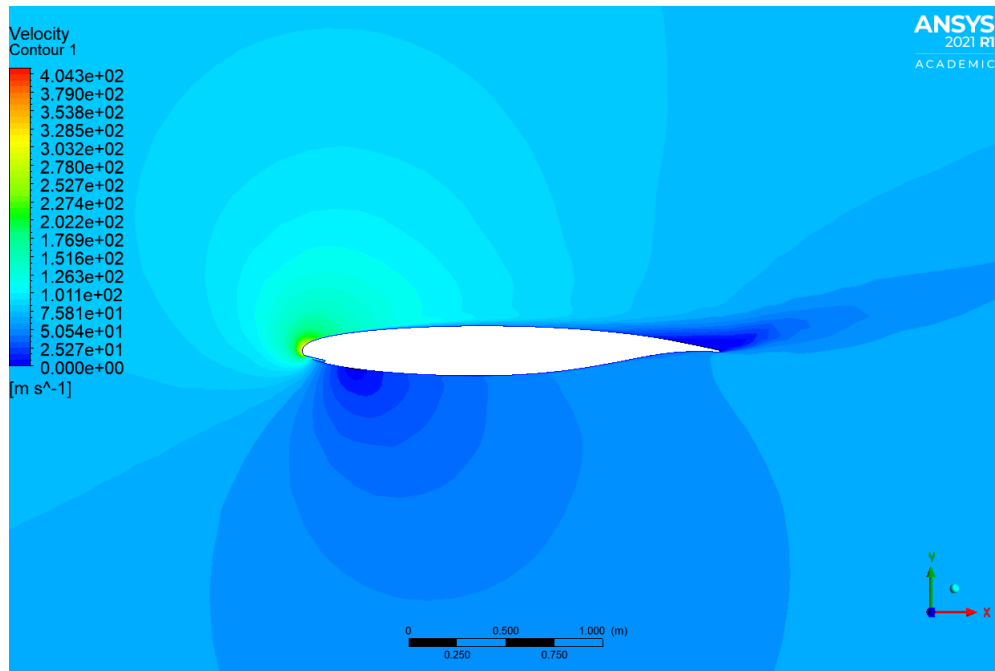Figure 26: Velocity field for 26° angle of attack with jet.

27

Figure 27: Velocity field for 26° angle of attack with jet.